vehicles

MDPI

Article

Ride Comfort Improvements on Disturbed Railroads Using Model Predictive Control

Alexander Posseckert * and Daniel Lüdicke

Institute of System Dynamics and Control, German Aerospace Center (DLR), Münchener Straße 20, 82234 Weßling, Germany; daniel.luedicke@dlr.de

* Correspondence: alexander.posseckert@dlr.de; Tel.: +49-8153-28-1740

Abstract: This paper proposes a control strategy for active lateral secondary suspension that uses preview data. Based on a derived analytical model, a model predictive controller (MPC) is implemented. The influence of the track irregularities upon carbody lateral dynamics is considered explicitly. The controller developed is applied to a full-scale rail vehicle model. Ride comfort is evaluated according to EN 12299. Multibody simulations show that there is a significant increase in continuous ride comfort on poor-quality tracks.

Keywords: railway vehicle; comfort; active suspension; MPC; preview; track irregularities

Citation: Posseckert, A.; Lüdicke, D. Ride Comfort Improvements on Disturbed Railroads Using Model Predictive Control. *Vehicles* **2023**, *5*, 1353–1366. https://doi.org/10.3390/vehicles5040074

Academic Editors: Pedro Aires Montenegro, Hugo Magalhães and Pedro Antunes

Received: 18 August 2023
Revised: 22 September 2023
Accepted: 5 October 2023
Published: 12 October 2023

1. Introduction

Railway transport will play an even more important role in future mobility because of its environmental friendliness. Along with this, a further increase in reliability, capacity, and attractiveness is inevitable. DLR's Next-Generation Train (NGT) project is investigating what future high-speed trains could look like [1–3]. Its main features are a lightweight, double-deck carbody design and a mechatronic running gear with Driven Independently Rotating Wheels (DIRW).

The increasing digitalization of the transport sector supports better communication and information processing. Today's modern signalling communication between train and infrastructure is characterised by communication-based train control systems such as ERTMS/ETCS [4]. Modern passenger trains, e.g., Siemens Velaro, already use mobile communications for business-related functions such as system health status, predictive maintenance or passenger information. Ethernet-based on-train communication networks are already specified in the IEC 61375 standard [5,6] and translated into national standards, e.g., EN 61375 [7]. The growth of available bandwidth and more flexibility enable new applications. Train communication network (TCN) innovations are being developed in Shift2Rail projects [8] and will be continued in ERJU projects [9]. With the increasing connectivity of rail transport in general, the availability of information about the train and its environment is also improving accordingly. Existing information from land-side databases, cloud services or other (preceding) trains can be transferred more easily and used more widely. For example, information about a train's current and future route enables mechatronic running gears to adapt to track conditions.

The running gear serves as a link between the track and the carbody of a railway vehicle. Its suspension carries the weight of the carbody, provides movement guidance and facilitates acceleration or braking [10]. During the ride, the wheel pairs experience track excitations due to routing and track deviations. However, the running gear must minimize the acceleration and jerk experienced by passengers in order to improve vibration comfort. Various suspension technologies have been developed to decouple track excitations from the carbody movement. The suspension systems can be broadly classified into passive, semi-active and active ones. A general overview regarding this research topic is given in [11–13]. (Semi-)active suspension has an actuation or control system that relies on sensor

data. With semi-active dampers, the damping rate can be adjusted and, thus, influence the dissipation of kinetic energy. Active spring-damper systems can absorb kinetic energy and also actively exert forces. Currently, passive and (semi-)active secondary suspension systems mostly aim to filter or dampen track irregularities experienced as stochastic effects in a reactive manner. The combination of new data sources enabled by digitalisation along with active suspension and innovative controllers opens up new potential for rail vehicles.

Model Predictive Control (MPC) is a promising control strategy for active suspension. Its main advantage lies in the ability to anticipate and compensate for future disturbances that impact the system. Furthermore, MPC can account for state restrictions or actuator limitations directly. Although MPC is adopted for active suspension in automotive research, e.g., [14–16], it is not commonly utilized for active suspension in railway technology. MPC is used to avoid hunting instability in railway vehicles. This is reported in [17] via the use of active yaw dampers. The use of DIRW in NGT's running gear design means that hunting instability is unlikely to occur. Another MPC-based approach was implemented in [18–20]. The studies only focus on vertical degrees of freedom, such as bouncing and pitching. Acceleration as well as suspension deflection can be successfully reduced; however, in order to evaluate comfort holistically, lateral motion has to be taken into account as well.

In order to improve ride comfort using active suspension, a detailed knowledge of track characteristics and their positions would be advantageous. The potential for improvement remains underexplored due to a lack of real-time track data, communication possibilities, and mechatronic actuators. In this regard, the present work outlines a control method for active lateral secondary suspension based on MPC. It is investigated how knowledge about the track ahead can be used for MPC in order to increase ride comfort.

Section 2 introduces the analytical model of the vehicle and the MPC control method based on it. Simulation results and the potential for improvement of the method are presented in Section 3. Section 4 provides further discussions of the results, followed by a summary in Section 5.

2. Modeling

This paper focuses on lateral dynamics; therefore, the following degrees of freedom (DOF) are considered for the carbody: Lateral displacement y_{cb}, roll angle ϕ_{cb} and yaw angle ψ_{cb}. In addition, each bogie is allowed to rotate around the x-axis by the angle $\phi_{bg,fr/re}$. This yields a model with 5 DOF, as illustrated in Figure 1. Note that a more detailed description is given in Figure A1.

$$\boldsymbol{q} = \begin{bmatrix} y_{cb} & \phi_{cb} & \phi_{bg,fr} & \phi_{bg,re} & \psi_{cb} \end{bmatrix}^T. \tag{1}$$

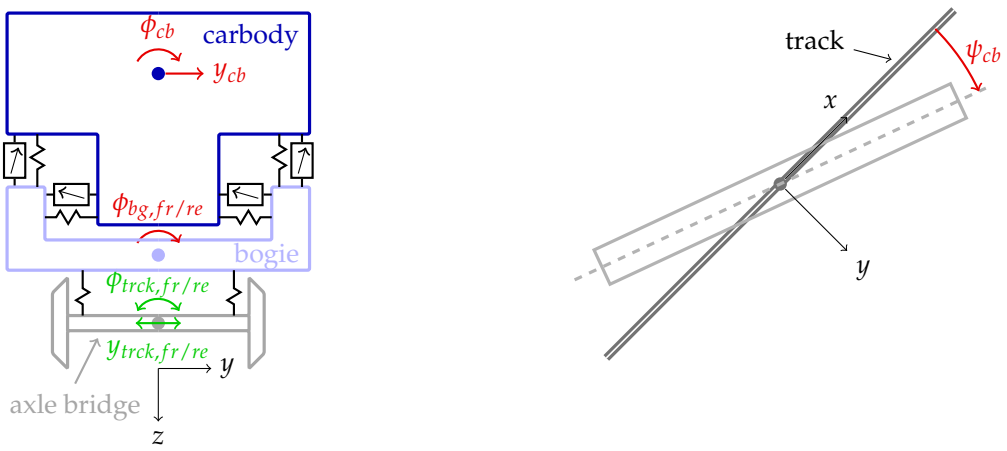

Figure 1. Definition degrees of freedom (red). Furthermore, the base excitation of the axle bridge due to track irregularities (green) is visualized. (**Left**) Cross section. (**Right**) Top view.

During the creation of the analytical model, track irregularities are considered explicitly. In order to achieve this, track errors are modelled as base excitation of the axle bridge; see Figure 1. The interaction between wheel and rail is simplified as follows. The running gear design of the NGT includes DIRW. While velocity-dependent hunting motion no longer applies, lateral guidance control is required in order to prevent flange contact; see [2]. The controller designed for this purpose significantly influences the axle bridge movement and, thus, the impact of track errors upon carbody dynamics. Figure 2 illustrates the step response of the axle bridge with respect to a lateral displacement. The result was obtained from a multibody simulation (MBS) of the NGT at a velocity of 120 km h^{-1}. In general, the response depends on velocity. In order to take this complex closed-loop behavior into account when creating the model, it is proposed to approximate the resulting lateral dynamics of the axle bridge via a transfer function. The algorithm used for the determination of the transfer function parameters is based on a least squares method; see [21]. It is found that a transfer function with a numerator degree of 1 and denominator degree of 2, as given in Equation (2), is sufficient to approximate the illustrated response; see Figure 2. To conclude, the axle bridge of the analytical model is excited by track irregularities which have been filtered through a velocity dependent transfer function.

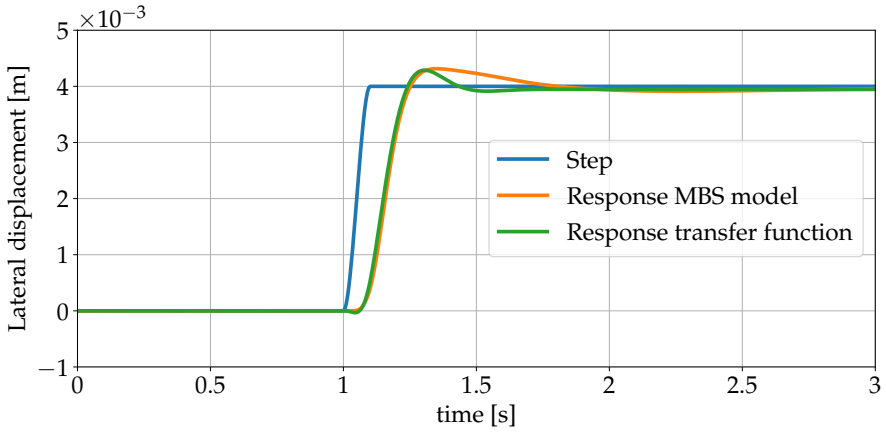

Figure 2. Step response for lateral displacement of the axle bridge. Orange: MBS model. Yellow: Derived model where the axle bride motion is simplified by a transfer function.

$$TF_{120} = \frac{-5.06\,s + 279.4}{s^2 + 20.5\,s + 283.2}. \tag{2}$$

The main focus of this work is lateral dynamics. Therefore, vertical components of track irregularities are disregarded. The remaining components of track excitation at both front and rear bogie are collected in the disturbance vector

$$\boldsymbol{z} = \begin{bmatrix} \phi_{trck,fr} & \dot{\phi}_{trck,fr} & \phi_{trck,re} & \dot{\phi}_{trck,re} & y_{trck,fr} & \dot{y}_{trck,fr} & y_{trck,re} & \dot{y}_{trck,re} \end{bmatrix}^T. \tag{3}$$

While deriving the equations of motion via Newton–Euler, the following additional assumptions are made:

- Due to the mechatronic guidance of NGT's running gear, flange contact does not occur.
- Bumpstop contact can be avoided since MPC has the ability to handle state restrictions (e.g., suspension deflections).
- Small angles of roll and yaw are assumed.

Based on these assumptions, the equations of motion can be linearized. A detailed description is given in Appendix A

$$\boldsymbol{M}\ddot{\boldsymbol{q}} + \boldsymbol{D}\dot{\boldsymbol{q}} + \boldsymbol{K}\boldsymbol{q} = \boldsymbol{F}_{act}\,\boldsymbol{u} + \boldsymbol{F}_{dist}\,\boldsymbol{z}. \tag{4}$$

Subsequently, the system is transformed into state space

$$\begin{aligned} \dot{\boldsymbol{x}} &= \boldsymbol{A}\boldsymbol{x} + \boldsymbol{B}\boldsymbol{u} + \boldsymbol{E}\boldsymbol{z} \\ \boldsymbol{y} &= \boldsymbol{C}\boldsymbol{x} \end{aligned} \tag{5}$$

with

$$\boldsymbol{x} = \begin{bmatrix} \boldsymbol{q} & \dot{\boldsymbol{q}} \end{bmatrix}^T. \tag{6}$$

In the secondary suspension, the actuators are mounted in both lateral and vertical directions; see Figure 1. Consequently, forces can be applied in the lateral direction as well as torques around the x and z-axis

$$\boldsymbol{u} = \begin{bmatrix} F_{lat} & M_{roll} & M_{yaw} \end{bmatrix}^T. \tag{7}$$

In the disturbance vector $\boldsymbol{z}$, the influence of track layout (e.g., centrifugal force in small radius curves) might be integrated as well; however, this paper focuses on disturbances due to track irregularities. The carbody DOF are chosen as output

$$\boldsymbol{y} = \begin{bmatrix} y_{cb} & \phi_{cb} & \psi_{cb} \end{bmatrix}^T. \tag{8}$$

Equation (5) is now transformed to discrete formulation with timestep k using the first-order hold method. Furthermore, control variable $\boldsymbol{u}$ can be written via its change in one timestep and its previous value; see Equation (9). Both formulations are equivalent, though it is easier to incorporate actuator dynamics later by restricting the change in each timestep

$$\boldsymbol{u}(k) = \boldsymbol{u}(k-1) + \Delta\boldsymbol{u}(k). \tag{9}$$

Finally, one obtains

$$\begin{aligned} \boldsymbol{x}(k+1) &= \boldsymbol{A}_d\boldsymbol{x}(k) + \boldsymbol{B}_d\boldsymbol{u}(k-1) + \boldsymbol{B}_d\Delta\boldsymbol{u}(k) + \boldsymbol{E}_d\boldsymbol{z}(k) \\ \boldsymbol{y}(k) &= \boldsymbol{C}_d\boldsymbol{x}(k). \end{aligned} \tag{10}$$

Using the model described in Equation (10), MPC minimizes a cost function J over the prediction horizon n_p by determining an optimal sequence of control variables over the control horizon n_c. Then, the first element of the sequence is applied and the process is repeated in the next timestep $k+1$, see [22]. When setting up the cost function, system output and control variables are collected in a single vector for the whole prediction horizon and control horizon, respectively

$$\bar{\boldsymbol{y}}(k+1) = \begin{bmatrix} \boldsymbol{y}(k+1) \\ \boldsymbol{y}(k+2) \\ \vdots \\ \boldsymbol{y}(k+n_p) \end{bmatrix}, \qquad \Delta\bar{\boldsymbol{u}}(k) = \begin{bmatrix} \Delta\boldsymbol{u}(k) \\ \Delta\boldsymbol{u}(k+1) \\ \vdots \\ \Delta\boldsymbol{u}(k+n_c-1) \end{bmatrix}. \tag{11}$$

The same is carried out for disturbances

$$\bar{\boldsymbol{z}}(k) = \begin{bmatrix} \boldsymbol{z}(k) \\ \boldsymbol{z}(k+1) \\ \vdots \\ \boldsymbol{z}(k+n_p-1) \end{bmatrix}. \tag{12}$$

The output prediction over the prediction horizon is given by

$$\bar{\boldsymbol{y}}(k+1) = \boldsymbol{F}\boldsymbol{x}(k) + \boldsymbol{G}\boldsymbol{u}(k-1) + \boldsymbol{S}\bar{\boldsymbol{z}}(k) + \boldsymbol{H}\Delta\bar{\boldsymbol{u}}(k), \tag{13}$$

where $\boldsymbol{F}$, $\boldsymbol{G}$, $\boldsymbol{S}$ and $\boldsymbol{H}$ can be derived from the system matrices; see Equation (A9). With weighting matrices $\boldsymbol{Q}$ and $\boldsymbol{R}$, the cost function J that has to be minimized can be formulated as

$$\begin{aligned} \min_{\Delta\bar{\boldsymbol{u}}(k)} \quad & J = \bar{\boldsymbol{y}}(k+1)^T \boldsymbol{Q} \bar{\boldsymbol{y}}(k+1) + \Delta\bar{\boldsymbol{u}}(k)^T \boldsymbol{R} \Delta\bar{\boldsymbol{u}}(k) \\ \text{s.t.} \quad & \Delta\boldsymbol{u}_{min} \leq \Delta\boldsymbol{u}(k) \leq \Delta\boldsymbol{u}_{max} \\ & \boldsymbol{y}_{min} \leq \boldsymbol{y}(k) \leq \boldsymbol{y}_{max}. \end{aligned} \tag{14}$$

3. Simulation Results

The derived controller is applied to a full-scale vehicle model of the NGT. Due to several of its main features (e.g., lightweight carbody design in doubledeck configuration) it has turned out to be challenging to achieve a sufficient ride comfort with conventional passive secondary suspension. Therefore, the vehicle offers an ideal platform for testing the controller. The simulation consists of two main parts. Multibody simulations are performed in the Simpack 2021.3 software. For the controller, a function has been written in Simulink (Matlab) based on the MPC realization described in [23]. The optimization problem is solved using Matlab 2019b command quadprog based on an interior-point algorithm [24]. Both software products are interconnected using the co-simulation interface Simat.

A track has been chosen that is comparable to EN 14363 test zone 1 [25], see Figure A2. In this scenario, track parameters like curvature and superelevation are not expected to have a significant influence upon lateral dynamics. Lateral and crosslevel track irregularities are chosen according to ERRI B176 high [26]. The standard deviation of lateral alignment Δy_σ^0 is 1.19 mm. At a speed of 120 km h^{-1}, this is within the target test range TL90 defined in EN 14363; see Table 1. For the crosslevel direction, no specifications are made in EN 14363. In addition, TL90 applies to the left and right rail separately, while ERRI B176 is for track-related excitations (i.e., for both rails at once). In order to ensure that the TL90 criterion for the longitudinal level Δz_σ^0 is not exceeded, no additional vertical track irregularities are used. For the selected crosslevel excitation, the standard deviation of vertical distance between the left and right rail is 2.12 mm. Therefore, the requirements of EN 14363 regarding track geometric quality are met; see Table 1. The evaluation of ride comfort is carried out according to EN 12299 [27]. This means the variable N_{MVy} is determined, which incorporates lateral acceleration measured at several positions on both floors of the carbody; see Figure 3.

Table 1. Track geometric quality: Target test ranges for standard deviation TL90 [25].

Reference Speed	Alignment Δy_σ^0	Longitudinal Level Δz_σ^0
$V \leq 120$ km h^{-1}	1.05–1.45 mm	1.80–2.50 mm

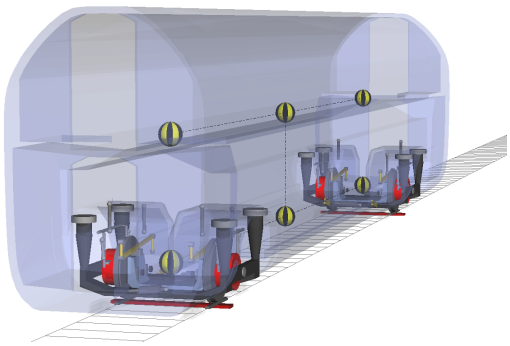

Figure 3. MBS model of a NGT middle wagon. Measurement points are visualized as yellow spheres.

Numerical results are presented in Figure 4. Note that only the lateral comfort index N_{MVy} is considered since this paper focuses on lateral dynamics. In order to evaluate ride comfort holistically, vertical and longitudinal motion has to be taken into account as well.

Compared to a model of the NGT with passive secondary suspension, a better ride comfort is achieved at all measurement points with MPC, recognizable by a lower N_{MVy} value. For instance, on the top deck at front sensor position there is an improvement of 47%. It is noticeable that at both center-measurement points, ride comfort is better compared to front and rear measurement points. At measurement point center bottom, for example, N_{MVy} value is only 30% of the one determined at rear bottom. When comparing ride comfort for the lower and upper floor, no larger differences are apparent.

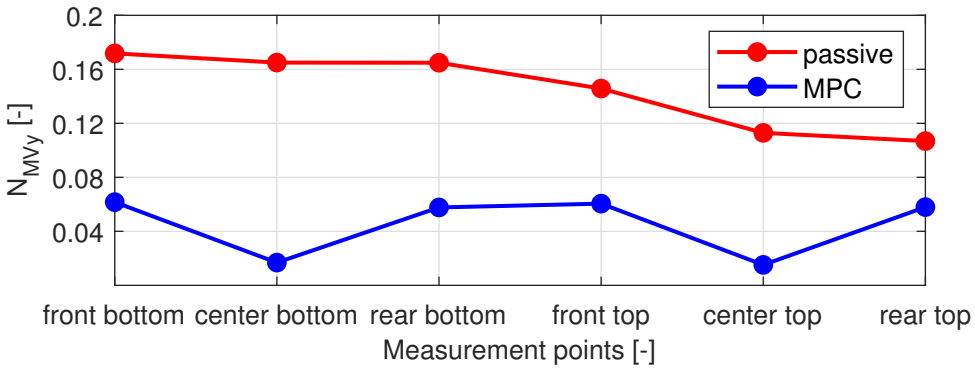

Figure 4. Lateral ride comfort index evaluated at different measurement points.

In order to predict future system behaviour, MPC requires the current train position. To obtain information regarding the required positioning accuracy, several simulations are carried out with different localization errors. For example, a test case is performed in which there is an intentional error of $+2\,\mathrm{m}$ in positioning between the actual train position and the assumed position fed into MPC. The results are given in Table 2. Lateral ride comfort obtained at two selected measurement points is given for different localization errors. Furthermore, the result of a simulation without knowledge of track data is listed as well, i.e., $\bar{\boldsymbol{z}}(k) = \mathbf{0}$. The far-right column compares test cases with localization errors to the reference case without errors. It can be observed that ride comfort deteriorates by 31% if the track ahead is not known. Nevertheless, even without track data the proposed active lateral suspension still provides better comfort than the passive system; see Figure 4. If positioning accuracy is less or equal $\pm 1.0\,\mathrm{m}$, results subjected to localization errors are better than the test case without track data. Finally, it is worth mentioning that N_{MVy} values for "positive" positioning errors are better than for the "negative" ones.

Table 2. Results for lateral comfort index when the determination of the train position is faulty.

Localization Error	NMVy Center Top	NMVy Rear Top	NMVy Rear Top Comparison to Error-Free
$+2.0\,\mathrm{m}$	0.038	0.086	41%
$+1.0\,\mathrm{m}$	0.030	0.071	16%
$+0.5\,\mathrm{m}$	0.021	0.063	3%
$\pm 0.0\,\mathrm{m}$	0.016	0.061	Reference
$-0.5\,\mathrm{m}$	0.022	0.067	9%
$-1.0\,\mathrm{m}$	0.031	0.078	28%
$-2.0\,\mathrm{m}$	0.039	0.099	62%
No track data	0.029	0.080	31%

Next, the energy consumption of all actuators mounted in a coach is considered. Assuming point-to-point force elements for the actuators shown in Figure 1, the directions of relative velocity v and applied forces F coincide; see [28]. Therefore, the current power P of each force element is determined using the scalar equation

$$P = F\,v. \tag{15}$$

By integrating power over time, the energy consumed by the actuators is obtained. Since EN 12299 prescribes measurement durations of 300 s, the time period is chosen accordingly. At a speed of 120 km h^{-1}, this corresponds to a track length of 10 km. Figure 5 shows the required power of a lateral actuator during simulation with peak values of approx. 80 W. In addition, negative values of power can be observed. This offers potential for recuperation.

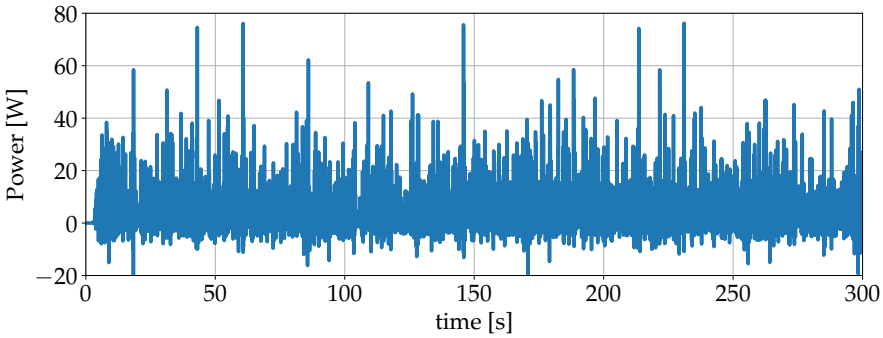

Figure 5. Power consumption of one lateral actuator during a test scenario.

The total energy summed up over all actuators of a coach is illustrated in Figure 6. For the considered track scenario, 4.5 W h of energy is consumed. For comparison, the same simulation is carried out using actuators with energy-harvesting capabilities. In this case, energy consumption is 3.9 W h, which corresponds to a reduction of 13%. Assuming an annual mileage of 500,000 km, the energy consumption for the reference case adds up to 225 kW h each year.

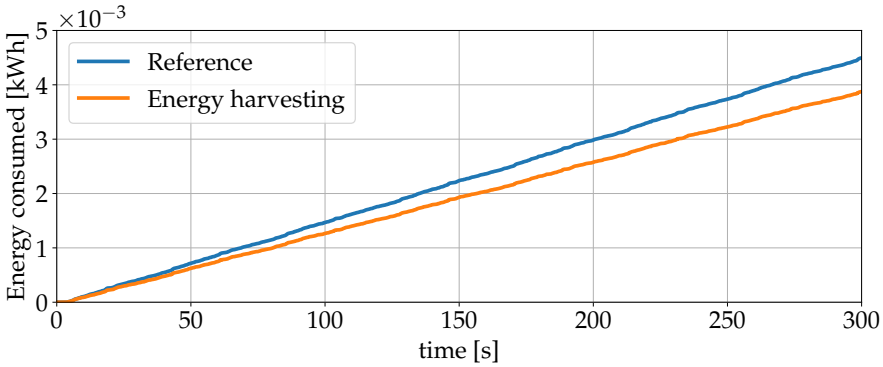

Figure 6. Consumed energy for all actuators of one coach during a test scenario. Blue: Reference case. Orange: Actuators with energy-harvesting capabilities.

4. Discussion

The results obtained in Section 3 indicate that the analytical model given in Equation (5) in combination with the assumed impact of irregularities is suitable for predicting future dynamic behaviour of the carbody. Using MPC, it was shown that, compared to a model of the NGT with passive secondary suspension, a significant increase in lateral ride comfort can be achieved; see Figure 4. It is noticeable that better N_{MVy} values are obtained near carbody's center of gravity compared to measurement points above the front and rear bogie. Consequently, ride comfort is significantly influenced by carbody yaw motion. In contrast to this, between the upper and lower floor no larger influence is detectable. Therefore, roll motion seems to be suppressed effectively.

In Table 2, the influence of positioning inaccuracy is examined. If the localization error is less or equal to ± 1 m, it is advantageous to consider the upcoming track in the control algorithm as shown in Equation (13). This behaviour is plausible since the effect of a single bump upon carbody dynamics is tied to a very specific location. Thus, if the

current train position is not located precisely, the future behaviour cannot be predicted well by MPC. This represents an ambitious requirement in terms of train localisation. However, for other applications like automatic train operation, precise and reliable train position data are necessary as well. Furthermore, the controller proposed in this paper is most effective on tracks with poor track quality that are not travel at high speeds. Therefore, it is likely that the required position accuracy needed for this application can be reached. Also, it is worth mentioning that even with larger errors in localization the proposed active lateral suspension still provides better ride comfort than the passive system. It is noticeable that lateral ride comfort for "positive" localization errors is better than for the "negative" ones; see Table 2. It is assumed that this asymmetry is based on the simplified modeling of NGTs lateral guidance control.

The requirements regarding power and energy usage of the actuators are quantified in Figures 5 and 6, respectively. The energy consumption required in order to counteract track irregularities is rather low compared to other consumers. However, especially on curvy tracks with high cant deficiency, lateral centering is a relevant part of active secondary suspension; see [29]. In order to investigate energy demand holistically, both needs to be considered together. Another important aspect is the requirements regarding actuator dynamics that must be fulfilled. In Figure 7, Fourier transform is applied to a signal that represents the force of a lateral actuator. Forces up to a frequency of 10 Hz can be observed. At a speed of 120 km h^{-1}, track excitation defined by ERRI high lies in this frequency range. While this was to be expected, it poses a challenging demand for the actuators. For example, in their studies on active secondary suspension, Orvnäs et al. used an electro-hydraulic actuator that only performed well up to 6 Hz; see [30]. However, the main goal of this paper is to provide a functional demonstration of MPC. Its suitability as a ride comfort controller has been proven. Lowering the required frequency range of the actuators by reducing controller gains or switching from active to semi-active suspension is an important issue which will be investigated further.

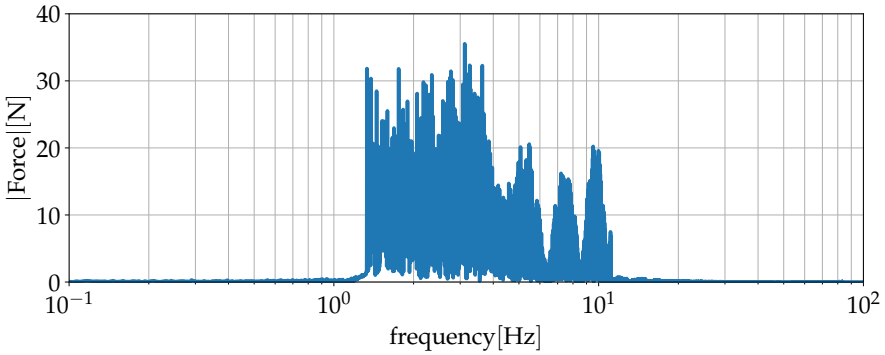

Figure 7. Force spectrum of one lateral actuator.

This paper focuses on minimizing the influence of track irregularities upon ride comfort. Using MPC, good results were obtained without considering wheel/rail-contact explicitly. Another important aspect is the influence of track layout upon carbody dynamics. It is expected that on tracks with small radius curves and high cant deficiency, there will be a non-negligible impact on ride comfort. In Section 2, it was mentioned that in the disturbance vector z, the influence of track layout (e.g., centrifugal force in small radius curves) might be integrated as well. To fully exploit the potential of MPC, both track irregularities and track layout should be considered.

5. Conclusions

A controller for active lateral secondary suspension based on Model Predictive Control (MPC) has been introduced in this paper. With the increase in digitalisation, the availability of information about the train and its environment is improving. This enables the opportunity to increase ride comfort by using information about the preceding track. To design the

controller, an analytical model which describes the carbody lateral dynamics is developed. The impact of track irregularities (in particular lateral and roll excitation) is considered explicitly. The controller is applied to a multibody simulation of the NGT on the tangent track and very large radius curves according to EN 14363. On the selected tracks, there is a significant improvement of ride comfort at each measurement point.

It was found that if the localisation error is less or equal to ± 1 m, it is advantageous to consider the upcoming track in the control algorithm. Since other applications like automatic train operation require precise and reliable train position data as well, it is expected that this accuracy can be reached. Furthermore, even without track data, the proposed active lateral suspension still provides better comfort than a comparable vehicle with passive secondary suspension.

The energy consumption of the actuators for the scenario considered is rather low. However, especially on curvy tracks with high cant deficiency, energy usage might increase. In order to investigate energy demand holistically, both scenarios need to be considered together. Furthermore, it is worth mentioning that the control method proposed in this paper puts high requirements on the actuator dynamics up to 10 Hz.

Multibody simulations of the NGT showed promising results. The next step is to incorporate a more detailed model of the actuators. Furthermore, an analysis of robustness of the controller is still pending. However, it is important to emphasize that a significant part of external disturbances that might affect the system are already considered in the disturbance vector $\boldsymbol{z}$.

Author Contributions: Conceptualization, A.P. and D.L.; methodology, A.P.; software, A.P. and D.L.; validation, A.P.; formal analysis, A.P.; investigation, A.P.; resources, A.P. and D.L.; data curation, A.P. and D.L.; writing—original draft preparation, A.P.; writing—review and editing, A.P. and D.L.; visualization, A.P.; supervision, A.P.; project administration, A.P. All authors have read and agreed to the published version of the manuscript.

Funding: This research received no external funding.

Institutional Review Board Statement: Not applicable.

Data Availability Statement: Not applicable.

Conflicts of Interest: The authors declare no conflict of interest.

Abbreviations

The following abbreviations are used in this manuscript:

NGT	Next-Generation Train.
TCN	Train communication network.
MPC	Model Predictive Control.
DIRW	Driven independently rotating wheels.
DOF	Degree of freedom.
w.r.t.	With respect to.
MBS	Multibody simulation
dist.	Distance
CoG	Center of gravity

Appendix A

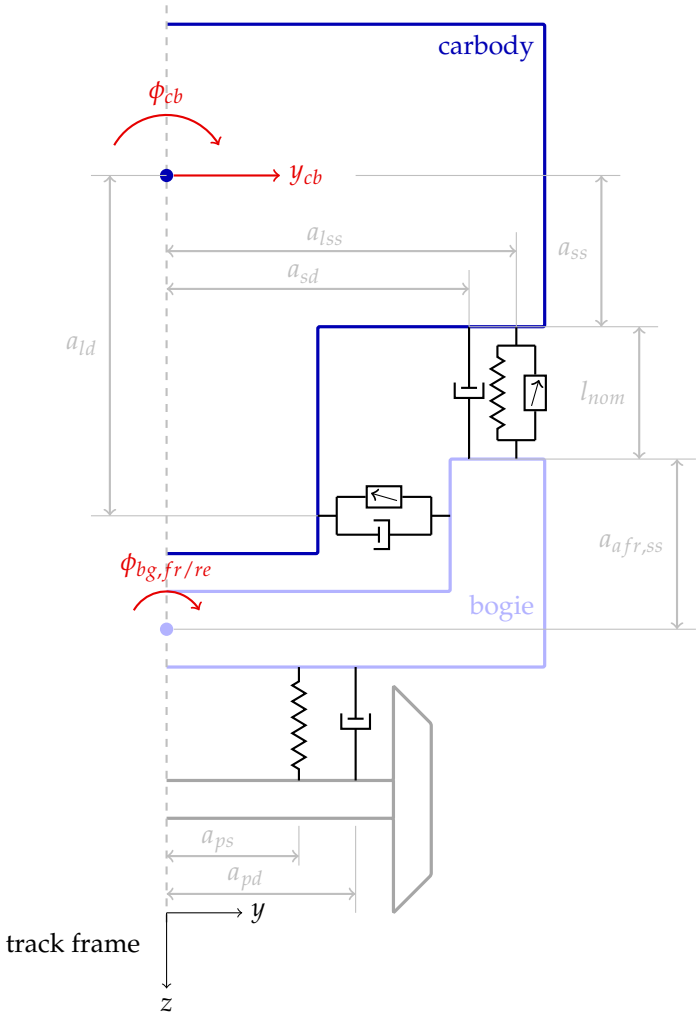

Figure A1. Detailed description of the derived model.

$$\boldsymbol{M} = \begin{bmatrix} m_{cb} & 0 & 0 & 0 & 0 \\ & I_{xx,cb} & 0 & 0 & 0 \\ & & I_{xx,bg} & 0 & 0 \\ \text{Sym.} & & & I_{xx,bg} & 0 \\ & & & & I_{zz,cb} \end{bmatrix} \tag{A1}$$

$$\boldsymbol{D} = \begin{bmatrix} d_{1,1} & d_{1,2} & 0 & 0 & 0 \\ & d_{2,2} & d_{2,3} & d_{2,4} & 0 \\ & & d_{3,3} & 0 & 0 \\ \text{Sym.} & & & d_{4,4} & 0 \\ & & & & d_{5,5} \end{bmatrix} \tag{A2}$$

$$\begin{aligned} d_{1,1} &= 4\,d_{ld} \\ d_{1,2} &= -\,4\,d_{ld}a_{ld} \\ d_{2,2} &= 4\,a_{ld}^2\,d_{ld} + 8\,a_{sd}^2\,d_{sd} \\ d_{2,3} &= -\,4\,a_{sd}^2\,d_{sd} \\ d_{2,4} &= -\,4\,a_{sd}^2\,d_{sd} \\ d_{3,3} &= 4\,a_{pd}^2\,d_{pd} + 2\,a_{ps}^2\,d_{z,ps} + 4\,a_{sd}^2\,d_{sd} \\ d_{4,4} &= 4\,a_{pd}^2\,d_{pd} + 2\,a_{ps}^2\,d_{z,ps} + 4\,a_{sd}^2\,d_{sd} \\ d_{5,5} &= 4\,d_{ld}\,a_{spd}^2 \end{aligned} \tag{A3}$$

$$\boldsymbol{K} = \begin{bmatrix} k_{1,1} & k_{1,2} & k_{1,3} & k_{1,4} & 0 \\ & k_{2,2} & k_{2,3} & k_{2,4} & 0 \\ & & k_{3,3} & 0 & k_{3,5} \\ \text{Sym.} & & & k_{4,4} & k_{4,5} \\ & & & & k_{5,5} \end{bmatrix} \tag{A4}$$

$$\begin{aligned} k_{1,1} &= 8\,c_y \\ k_{1,2} &= -\,8\,a_{ss}c_y - 8\,c_{y\phi} \\ k_{1,3} &= -\,4\,a_{afr,ss}\,c_y - 4\,c_{y\phi} \\ k_{1,4} &= -\,4\,a_{afr,ss}\,c_y - 4\,c_{y\phi} \\ k_{2,2} &= 8\,a_{lss}^2\,c_z + 8\,a_{ss}^2\,c_y - 8\,F_{pre}\,a_{ss} + 16\,a_{ss}\,c_{y\phi} + 8\,c_\phi \\ k_{2,3} &= 4\,a_{afr,ss}\,a_{ss}\,c_y - 4\,a_{lss}^2\,c_z + 4\,a_{afr,ss}\,c_{y\phi} + 4\,a_{ss}\,c_{y\phi} + 4\,l_{nom}\,c_{y\phi} - 4\,c_\phi \\ k_{2,4} &= 4\,a_{afr,ss}\,a_{ss}\,c_y - 4\,a_{lss}^2\,c_z + 4\,a_{afr,ss}\,c_{y\phi} + 4\,a_{ss}\,c_{y\phi} + 4\,l_{nom}\,c_{y\phi} - 4\,c_\phi \\ k_{3,3} &= 4\,a_{afr,ss}^2\,c_y + 4\,a_{lss}^2\,c_z + 2\,a_{ps}^2\,c_{z,ps} - 4\,F_{pre}\,a_{afr,ss} + 8\,a_{afr,ss}\,c_{y\phi} + 4\,c_\phi \\ k_{3,5} &= -\,4\,a_{afr,ss}\,a_{spd}\,c_y - 4\,a_{spd}\,c_{y\phi} \\ k_{4,4} &= 4\,a_{afr,ss}^2\,c_y + 4\,a_{lss}^2\,c_z + 2\,a_{ps}^2\,c_{z,ps} - 4\,F_{pre}\,a_{afr,ss} + 8\,a_{afr,ss}\,c_{y\phi} + 4\,c_\phi \\ k_{4,5} &= 4\,a_{afr,ss}\,a_{spd}\,c_y + 4\,a_{spd}\,c_{y\phi} \\ k_{5,5} &= 8\,c_y\,a_{spd}^2 \end{aligned} \tag{A5}$$

$$\boldsymbol{F}_{act} = \begin{bmatrix} -1 & 0 & 0 \\ a_{ld} & 1 & 0 \\ 0 & -0.5 & 0 \\ 0 & -0.5 & 0 \\ 0 & 0 & 1 \end{bmatrix} \tag{A6}$$

$$\boldsymbol{F}_{dist} = \begin{bmatrix} 0 & 0 & 0 & 0 & f_{1,5} & f_{1,6} & f_{1,7} & f_{1,8} \\ 0 & 0 & 0 & 0 & f_{2,5} & f_{2,6} & f_{2,7} & f_{2,8} \\ f_{3,1} & f_{3,2} & 0 & 0 & f_{3,5} & 0 & 0 & 0 \\ 0 & 0 & f_{4,3} & f_{4,4} & 0 & 0 & f_{4,7} & 0 \\ 0 & 0 & 0 & 0 & f_{5,5} & f_{5,6} & f_{5,7} & f_{5,8} \end{bmatrix} \tag{A7}$$

$$\begin{aligned} &f_{1,5} = 4\,c_y, && f_{1,6} = 2\,d_{ld} && f_{1,7} = 4\,c_y && f_{1,8} = 2\,d_{ld} \\ &f_{2,5} = -4\,c_y\,a_{ss} - 4\,c_{y\phi} && f_{2,6} = -2\,d_{ld}\,a_{ld} && f_{2,7} = -4\,c_y\,a_{ss} - 4\,c_{y\phi} && f_{2,8} = -2\,d_{ld}\,a_{ld} \\ &f_{3,1} = 2\,c_{z,ps}\,a_{ps}^2 && f_{3,2} = 4\,d_{pd}\,a_{pd}^2 + 2\,d_{z,ps}\,a_{ps}^2 && f_{3,5} = -4\,c_y\,a_{afr,ss} - 4\,c_{y\phi} && \\ &f_{4,3} = 2\,c_{z,ps}\,a_{ps}^2 && f_{4,4} = 4\,d_{pd}\,a_{pd}^2 + 2\,d_{z,ps}\,a_{ps}^2 && f_{4,7} = -4\,c_y\,a_{afr,ss} - 4\,c_{y\phi} && \\ &f_{5,5} = 4\,c_y\,a_{spd} && f_{5,6} = 2\,d_{ld}\,a_{spd} && f_{5,7} = -4\,c_y\,a_{spd} && f_{5,8} = -2\,d_{ld}\,a_{spd} \end{aligned} \tag{A8}$$

Table A1. Name and description of parameters that are used in connection with the analytical model.

Name	Description
m_{cb}	Carbody mass
$I_{xx,cb}$	Moment of inertia around x-axis, carbody
$I_{zz,cb}$	Moment of inertia around z-axis, carbody
$I_{xx,bg}$	Moment of inertia around x-axis, bogie
c_y	Lateral stiffness secondary suspension
c_z	Vertical stiffness secondary suspension
c_ϕ	Bending stiffness secondary suspension
$c_{y\phi}$	Cross-coupling stiffness secondary suspension
$c_{z,ps}$	Vertical stiffness primary suspension
d_{ld}	Lateral damping secondary suspension
d_{sd}	Vertical damping secondary suspension
d_{pd}	Vertical damping primary dampers
d_{ps}	Vertical damping primary suspension
a_{lss}	Half the distance between secondary springs
a_{sd}	Half the distance between secondary dampers
a_{ps}	Half the distance between primary springs
a_{pd}	Half the distance between primary dampers
a_{spd}	Half the distance between the center pivots
a_{ld}	Vertical dist. lateral damper to carbody CoG
a_{ss}	Vertical dist. secondary spring to carbody CoG
$a_{afr,ss}$	Vertical dist. bogie CoG to secondary spring
l_{nom}	Nominal length secondary springs
F_{pre}	Preload of secondary springs due to carbody mass

Appendix B

$$\boldsymbol{F} = \begin{bmatrix} \boldsymbol{CA} \\ \boldsymbol{CA}^2 \\ \boldsymbol{CA}^3 \\ \vdots \\ \boldsymbol{CA}^{n_p} \end{bmatrix}, \qquad \boldsymbol{G} = \begin{bmatrix} \boldsymbol{CB} \\ \boldsymbol{C}(\boldsymbol{A}+\boldsymbol{I})\boldsymbol{B} \\ \boldsymbol{C}\left(\boldsymbol{A}^2+\boldsymbol{A}+\boldsymbol{I}\right)\boldsymbol{B} \\ \vdots \\ \boldsymbol{C}\left(\boldsymbol{A}^{n_p-1}+\ldots+\boldsymbol{I}\right)\boldsymbol{B} \end{bmatrix}$$

$$\boldsymbol{H} = \begin{bmatrix} \boldsymbol{CB} & \boldsymbol{0} & \cdots & \boldsymbol{0} \\ \boldsymbol{C}(\boldsymbol{A}+\boldsymbol{I})\boldsymbol{B} & \boldsymbol{CB} & \cdots & \boldsymbol{0} \\ \boldsymbol{C}\left(\boldsymbol{A}^2+\boldsymbol{A}+\boldsymbol{I}\right)\boldsymbol{B} & \boldsymbol{C}(\boldsymbol{A}+\boldsymbol{I})\boldsymbol{B} & \cdots & \boldsymbol{0} \\ \vdots & \vdots & \ddots & \vdots \\ \boldsymbol{C}\left(\boldsymbol{A}^{n_c-1}+\ldots+\boldsymbol{I}\right)\boldsymbol{B} & \boldsymbol{C}\left(\boldsymbol{A}^{n_c-2}+\ldots+\boldsymbol{I}\right)\boldsymbol{B} & \cdots & \boldsymbol{CB} \\ \boldsymbol{C}(\boldsymbol{A}^{n_c}+\ldots+\boldsymbol{I})\boldsymbol{B} & \boldsymbol{C}\left(\boldsymbol{A}^{n_c-1}+\ldots+\boldsymbol{I}\right)\boldsymbol{B} & \cdots & \boldsymbol{C}(\boldsymbol{A}+\boldsymbol{I})\boldsymbol{B} \\ \vdots & \vdots & \ddots & \vdots \\ \boldsymbol{C}\left(\boldsymbol{A}^{n_p-1}+\ldots+\boldsymbol{I}\right)\boldsymbol{B} & \boldsymbol{C}\left(\boldsymbol{A}^{n_p-2}+\ldots+\boldsymbol{I}\right)\boldsymbol{B} & \cdots & \boldsymbol{C}\left(\boldsymbol{A}^{n_p-n_c}+\ldots+\boldsymbol{I}\right)\boldsymbol{B} \end{bmatrix} \tag{A9}$$

$$\boldsymbol{S} = \begin{bmatrix} \boldsymbol{CE} & \boldsymbol{0} & \boldsymbol{0} & \cdots & \boldsymbol{0} \\ \boldsymbol{CAE} & \boldsymbol{CE} & \boldsymbol{0} & \cdots & \boldsymbol{0} \\ \boldsymbol{CA}^2\boldsymbol{E} & \boldsymbol{CAE} & \boldsymbol{CE} & \cdots & \boldsymbol{0} \\ \vdots & \vdots & \vdots & \ddots & \vdots \\ \boldsymbol{CA}^{n_p-1}\boldsymbol{E} & \boldsymbol{CA}^{n_p-2}\boldsymbol{E} & \boldsymbol{CA}^{n_p-3}\boldsymbol{E} & \cdots & \boldsymbol{CE} \end{bmatrix}$$

Appendix C

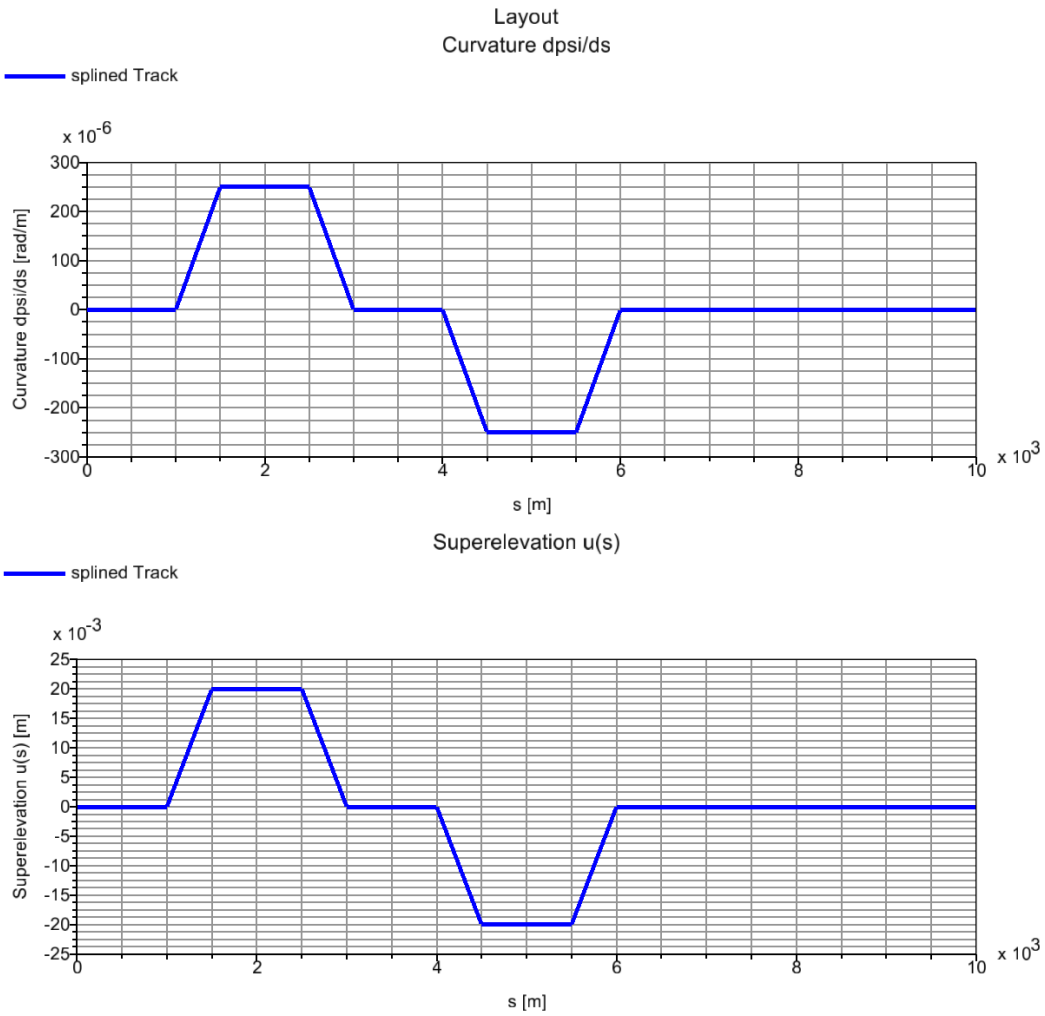

Figure A2. Track scenario.

References

1. Winter, J. Novel Rail Vehicle Concepts for a High Speed Train: The Next Generation Train. In Proceedings of the First International Conference on Railway Technology: Research, Development and Maintenance, Las Palmas de Gran Canaria, Spain, 18–20 April 2012; Civil-Comp Proceedings; Pombo, J., Ed.; Civil-Comp Press: Stirlingshire, UK, 2012. [CrossRef]
2. Heckmann, A.; Keck, A.; Grether, G. Active Guidance of a Railway Running Gear with Independently Rotating Wheels. In Proceedings of the 2020 IEEE Vehicle Power and Propulsion Conference (VPPC), Piscataway, NJ, USA, 18 November–16 December 2020; pp. 1–5. [CrossRef]
3. Heckmann, A.; Lüdicke, D.; Keck, A.; Goetjes, B. A Research Facility for the Next Generation Train Running Gear in True Scale. In *Advances in Dynamics of Vehicles on Roads and Tracks II*; Lecture Notes in Mechanical Engineering; Orlova, A., Cole, D., Eds.; Springer International Publishing: Cham, Switzerland, 2022; Volume 9, pp. 18–27. [CrossRef]
4. European Union Agency for Railways. Technical Specifications for Interoperability—Control Command and Signalling. Technical Report CCS. Available online: https://www.era.europa.eu/domains/technical-specifications-interoperability/control-command-and-signalling-tsi_en (accessed on 27 May 2016).
5. Ludicke, D.; Lehner, A. Train Communication Networks and Prospects. *IEEE Commun. Mag.* **2019**, *57*, 39–43. [CrossRef]
6. International Electrotechnical Commission. *Electronic Railway Equipment—Train communication Network (TCN)—Part 1: General Architecture*. Technical Report 61375-1; International Electrotechnical Commission: Geneva, Switzerland, 2012.
7. *DIN EN 61375-1:2015-02, Elektronische Betriebsmittel für Bahnen—Zug-Kommunikations-Netzwerk (TCN)—Teil 1: Allgemeiner Aufbau (IEC 61375-1:2012); Deutsche Fassung EN 61375-1:2012*; Technical Report; Deutsches Institut für Normung e.V.: Berlin, Germany, 2015. [CrossRef]
8. Shift2Rail CONNECTA. Final Report on the Contribution of CONNECTA to Shift2Rail: Deliverable D8.3. Available online: https://projects.shift2rail.org/download.aspx?id=e489bd37-4ec1-4fbf-bd1d-818bb0fc0762 (accessed on 14 August 2023).
9. Europe's Rail. Home—Europe's Rail. Available online: https://rail-research.europa.eu/ (accessed on 14 August 2023).

10. Schindler, C.; Brandhorst, M.; Dellmann, T.; Haigermoser, A.; Hecht, M.; Karch, S.; Löffler, G.; Rösch, W. (Eds.) *Handbuch Schienenfahrzeuge: Entwicklung, Produktion, Instandhaltung*, 1. auflage ed.; Eurail Press: Hamburg, Germany, 2014.
11. Fu, B.; Giossi, R.L.; Persson, R.; Stichel, S.; Bruni, S.; Goodall, R. Active suspension in railway vehicles: A literature survey. *Railw. Eng. Sci.* **2020**, *28*, 3–35. [CrossRef]
12. Qazizadeh, A. On Active Suspension in Rail Vehicles. Ph.D. Thesis, KTH Royal Institute of Technology, Stockholm, Sweden, 2017.
13. Orvnäs, A. *Methods for Reducing Vertical Carbody Vibrations of a Rail Vehicle: A literature Survey*; Järnvägsgruppen, KTH Railway Group: Stockholm, Sweden, 2010.
14. Gohrle, C.; Wagner, A.; Schindler, A.; Sawodny, O. Active suspension controller using MPC based on a full-car model with preview information. In Proceedings of the 2012 American Control Conference (ACC), Montreal, QC, Canada, 27–29 June 2012; pp. 497–502. [CrossRef]
15. Durmaz, B.E.; Kaçmaz, B.; Mutlu, İ.; Söylemez, M.T. Implementation and comparison of LQR-MPC on active suspension system. In Proceedings of the 2017 10th International Conference on Electrical and Electronics Engineering (ELECO), Bursa, Turkey, 30 November–2 December 2017; pp. 828–835.
16. Cho, B.K. Active suspension controller design using MPC with preview information. *KSME Int. J.* **1999**, *13*, 168–174. [CrossRef]
17. Chen, Y.; Wang, K.; Wang, Y.; Li, G. Model predictive control of active yaw damper for high-speed trains. In Proceedings of the Sixth International Conference on Traffic Engineering and Transportation System (ICTETS 2022), Guangzhou, China, 23–25 September 2022; Proceedings of SPIE; Zhou, J., Sheng, J., Eds.; SPIE: Bellingham, WA, USA, 2023; p. 140. [CrossRef]
18. Orukpe, P.E.; Zheng, X.; Jaimoukha, I.M.; Zolotas, A.C.; Goodall, R.M. Model predictive control based on mixed H_2/H_∞ control approach for active vibration control of railway vehicles. *Veh. Syst. Dyn.* **2008**, *46*, 151–160. [CrossRef]
19. Orukpe, P.E. Model Predictive Control Application to Flexible-Bodied Railway Vehicles for Vibration Suppression. *Int. J. Eng. Res. Afr.* **2013**, *10*, 25–35. [CrossRef]
20. Ulum, Z.; Affaf, M.; Salmah; Suparwanto, A. Active suspension systems design of a light rail vehicle using MPC with preview information disturbance. In Proceedings of the 2017 5th International Conference on Instrumentation, Control, and Automation (ICA), Yogyakarta, Indonesia, 9–11 August 2017; pp. 18–23. [CrossRef]
21. Ljung, L. *System Identification: Theory for the User*, 9th ed.; Prentice-Hall PTR information and system sciences series; Prentice-Hall PTR: Upper Saddle River, NJ, USA, 1996.
22. Borrelli, F.; Bemporad, A.; Morari, M. *Predictive Control for Linear and Hybrid Systems*; Cambridge University Press: Cambridge, UK; New York, NY, USA; Port Melbourne, Australia, 2017.
23. Adamy, J. *Nichtlineare Regelungen*; Springer: Berlin/Heidelberg, Germany, 2009. [CrossRef]
24. Coleman, T.F.; Li, Y. A Reflective Newton Method for Minimizing a Quadratic Function Subject to Bounds on Some of the Variables. *SIAM J. Optim.* **1996**, *6*, 1040–1058. [CrossRef]
25. *DIN EN 14363:2022-10, Bahnanwendungen—Versuche und Simulationen für die Zulassung der fahrtechnischen Eigenschaften von Eisenbahnfahrzeugen—Fahrverhalten und stationäre Versuche; Deutsche Fassung EN 14363:2016+A1:2018+A2:2022*; Technical Report; Deutsches Institut für Normung e.V.: Berlin, Germany, 2022. [CrossRef]
26. *ORE B 176. Bogies with steered or steering wheelsets. Report No. 1: Specifications and Preliminary Studies, Vol. 2. Specification for a Bogie with Improved Curving Characteristics*; Technical Report; Office for Research and Experiments (ORE): Utrecht, The Netherlands, 1989.
27. *DIN EN 12299:2009-08, Bahnanwendungen—Fahrkomfort für Fahrgäste; Deutsche Fassung EN 12299:2009*; Technical Report; Deutsches Institut für Normung e.V.: Berlin, Germany, 2009. [CrossRef]
28. Rill, G.; Schaeffer, T.; Borchsenius, F. *Grundlagen und computergerechte Methodik der Mehrkörpersimulation: Vertieft in Matlab-Beispielen, Übungen und Anwendungen*, 4. auflage ed.; Springer eBook Collection; Springer Vieweg: Wiesbaden/Heidelberg, Germany, 2020. [CrossRef]
29. Posseckert, A.; Lüdicke, D. Ride comfort improvements in switches using active secondary suspension with preview. In Proceedings of the Fifth International Conference on Railway Technology: Research, Development and Maintenance, Montpellier, France, 22–25 August 2022; Civil-Comp Conferences; Pombo, J., Ed.; Civil-Comp Press: Edinburgh, UK, 2023; pp. 1–6. [CrossRef]
30. Orvnäs, A.; Stichel, S.; Persson, R. Active lateral secondary suspension with H_∞ control to improve ride comfort: Simulations on a full-scale model. *Veh. Syst. Dyn.* **2011**, *49*, 1409–1422. [CrossRef]